Journal of EARTHQUAKE AND TSUNAMI

Managing Editors

Fook Hou Lee
National University of Singapore

Hori Muneo
Japan Agency for Marine-Earth Science and Technology, Japan

Zhenhua Huang
School of Ocean and Earth Science and Technology University of Hawaii at Manoa

World Scientific

Journal of Earthquake and Tsunami
(2021)

DOI: 10.1142/S179343112150010X

Surface Ground Movement Around a Steel Pipe Pile Foundation During Liquefaction Measured by Effective Stress Analysis

Nguyen Thanh Trung
University of Transport and Communications
Cau Giay, Dong Da, Hanoi, Vietnam
nttrung@utc.edu.vn

Dinh Quang Cuong*
Institute of Construction for Offshore Engineering
National University of Civil Engineering
55 Giai Phong, Hanoi, Vietnam
cuongdq@nuce.edu.vn

Osamu Kiyomiya
Coastal Development Institute of Technology (CDIT)
1-14-2 Nishi-Shimbashi, Minato-Ku, Tokyo 105-0003, Japan
kiyomiya@cdit.or.jp

Received 19 February 2020
Accepted 18 September 2020
Published 24 November 2020

Several studies on liquefaction using physical model tests and numerical analysis have been conducted in recent years; however, few studies have investigated the effect of liquefaction-induced settlement on structures. Especially, this settlement seriously influences on gravity foundation during earthquake. This study aims to investigate the settlement of the surrounding ground of steel pipe sheet pile (SPSP) foundation during liquefaction by using an effective stress analysis. 2D numerical modeling was used in this study and the behavior of undrained soil was idealized using a cocktail glass model. The numerical results were compared with experimental results from a 1-G shaking table test with a scale of 1:60. The results indicate that the settlement of surface ground and SPSP foundation rapidly increase when the liquefaction occurs and is significantly influenced by permeability coefficient of ground.

Keywords: Steel pipe sheet pile foundation; liquefaction; settlement; effective stress analysis; shaking table test.

1. Introduction

Damages to foundation structures and superstructures have been observed in liquefaction areas after past earthquakes, especially in the strong earthquake in

*Corresponding author.

Niigata in 1964 as reported by Kawakami and Asada [1966]. Most of these failures were due to the lateral spreading movement of liquefiable layer; however, several significant failures were caused by liquefaction-induced settlement after the earthquake. This settlement is caused by the dissipation of pore water pressures and is accompanied by a strain volume change and changes to the permeability of the soil layer. Kim *et al.* [2009] studied a dissipation model of pore water pressure in liquefied sandy ground; this study presented the combined process between the solidification of sand grains and the consolidation of the solidified layer. Shahir *et al.* [2012] and Wang *et al.* [2011] evaluated the effects of permeability and its changes during liquefaction and post liquefaction. The variation of permeability can be expressed as a function of pore water pressure, and the generation of pore water pressure and the drainage of pore water occur simultaneously. As a result, estimating the settlement during liquefaction is difficult. At present, the settlement is generally determined using a semi-empirical method, a dynamic effective stress analysis (ESA) and a vibration test.

The semi-empirical method is a simplified procedure, with the settlement calculated using the thickness of sub-layers and their volumetric strain after an earthquake. Tokimatsu and Seed [1984, 1987] set up charts to estimate cyclic volumetric strains in saturated sands using cyclic triaxial and simple shear tests and to evaluate settlements in sand due to earthquake shaking. Ishihara and Yoshimine [1992] estimated the volumetric strain based on resistance to liquefaction and relative density, and the results were adjusted by SPT blow counts and/or CPT tip resistance. Shamoto *et al.* [1998] developed a method based on a torsional shear test. Wu and Seed [2004] proposed an estimation of liquefaction-induced ground settlement and compared it with previous studies. Cetin *et al.* [2009a, 2009b] predicted the settlement after an earthquake using a probabilistic method with earthquake case histories. This approach modeled the nature of soil settlement and produced a smaller error compared with the previous studies.

ESA is one of the most advanced numerical analyses in geotechnical engineering. It simulates the complex dynamic behavior of soils in strong earthquakes during liquefaction related to the generation and dissipation of pore water pressure. Recently, two theory models of soil elements suggested by Iai *et al.* [1991, 2011] were adopted in seismic design work for the evaluation of liquefaction. The first one was originally suggested by Iai [1991] as a multi spring model in the undrained condition. Then, the second model was also improved by Iai *et al.* [2011], which was named as a glass cocktail model in the drained condition. These advanced models were used in FEM programs to model the behavior of the ground with many types of foundation structures during liquefaction and post-liquefaction. Wang *et al.* [2008] investigated the seismic behaviors of inclined micro-piles during liquefaction using Multi-spring models. Ueda *et al.* [2008] also used the model in modeling the seismic behavior of a self-supported sheet pile wall. Yoshida *et al.* [2012] investigated the effect of seismic reinforcement on a sheet pile quay wall by using a strain space multiple mechanism model for a soil element. Alchamaa [2010] conducted both experimental and

numerical methods to assess the post liquefaction deformation with seepage due to pore water pressure after an earthquake for a shallow foundation. Trung *et al.* [2014] also modeled the dynamic behavior of steel pipe sheet pile (SPSP) foundation in a liquefied layer during an earthquake. In this study, the effect of the ground slope on the dynamic responses of this foundation was evaluated during liquefaction by determining its dynamic responses using both the shaking table test and the numerical method.

The SPSP foundation structure is generally applied to long-span cable-stayed bridges crossing deep rivers and/or in poor soil conditions. This foundation works not only as a supporting structure but also as a retaining wall during liquefaction, the seepage flows may be restrained in the direction of the foundation. The dynamic behavior of the surrounding ground and foundation is complicated in strong earthquakes. Therefore, this study aims to further investigate the settlement of the surface ground and an SPSP foundation during liquefaction by using a numerical method and comparing with a vibration test. The ESA using a new advanced cocktail glass model was used in this study.

2. Shaking Table Test

The experimental test uses a 1-G shaking table facility of the Penta-Ocean Construction Corporation in Japan. The test is described as follows:

2.1. *Test model and material properties*

The prototype of test model is a tower-foundation system of a cable-stayed bridge supported by the SPSP foundation on the ground.

The foundation has 165 steel pipe piles with dimensions of 36.456 m length and 29.469 m width. Each steel pipe pile has a diameter of 150 cm and a thickness of 2.5 cm, as shown in Fig. 1. To simplify the structure for constructing the physical model, the superstructure-tower system of the prototype was modeled as a single degree of freedom system. The mass of the system includes the mass of the superstructure and tower at the top of the column. The natural frequency of the system was calculated as suggested by Yoneda [1990].

All material properties of the physical model and ground were scaled using a similitude law suggested by Iai [1988]. Table 1 summarizes the scaling factors applied in this shaking model test.

The test model includes the pier, superstructure, and foundation in the sandy ground. The natural frequency of the pier-superstructure system of the model was determined by the dynamic characteristics of the single-degree-of-freedom system of the prototype using a scale of 1:60. The pier in the model consists of four steel columns that are rigidly fixed together by a steel plate at the top with a mass of 60 kg. Each column has dimensions of 1.1 m height and a cross-section in a tubular shape of 2.27 cm diameter and 0.19 cm thickness. The foundation is a caisson made of

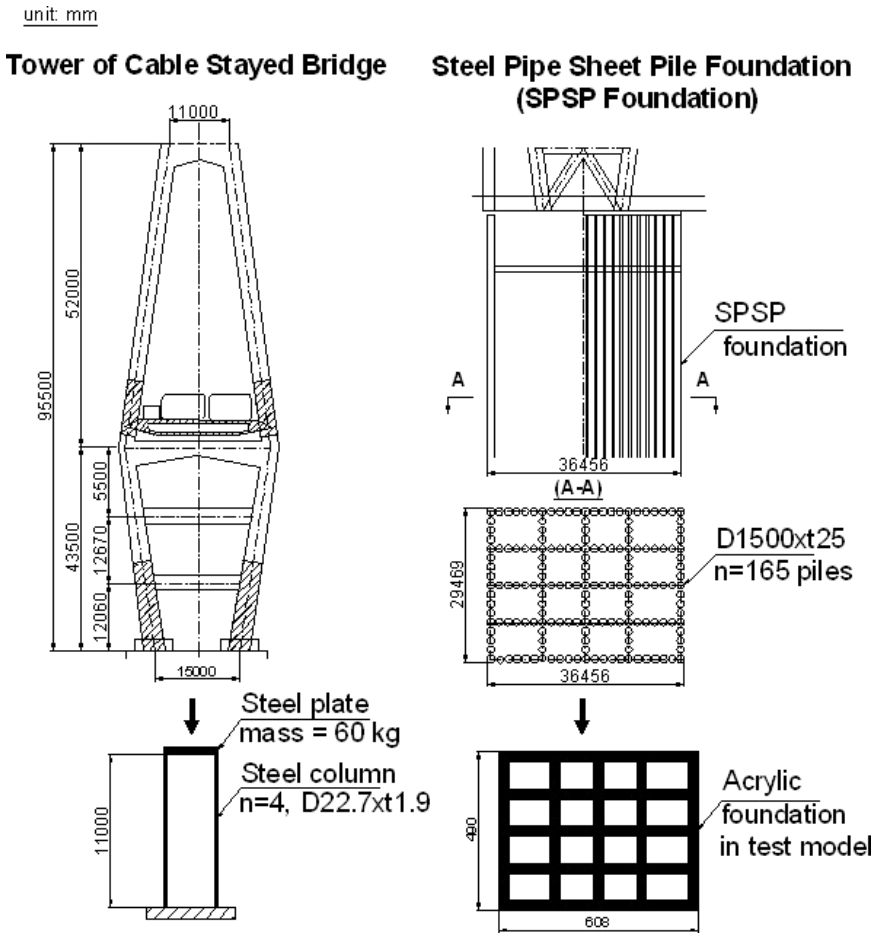

Fig. 1. Cable stayed bridge prototype.

acrylic materials with dimensions of 49 cm width, 60.8 cm length, and 83.4 cm height. The cap at the top of the foundation is an acrylic plate that is 60.8 cm long, 49 cm wide, and 9.8 cm thick. The footing of the pier is constructed of steel with dimensions of 26.6 cm length, 46.6 cm width, and 18.5 cm thickness.

The ground in the models consists of a 48.8 cm liquefiable sand layer with a relative density of 50% using Yamagata sand No. 6 ($D_{50} = 0.3$ mm) overlying a 74.3 cm non-liquefiable layer with a relative density of 90%. The soil layers of the model ground were constructed using the sand drop method. The sand was gradually dropped into the vessel up to the water level step. However, the relative density of the non-liquefiable layer was controlled by the amount of tamping and the measured weight of the sand layer. The thickness of the sand layer for each tamping period was 10 cm.

Table 1. Scaling factors of the shaking model test.

Parameter	λ = prototype/model	Scale
Length	λ	60
Density	1	1
Time	$\lambda^{0.75}$	21.56
Stress	λ	60
Pore water pressure	λ	60
Displacement	$\lambda^{1.5}$	464.76
Acceleration	1	1
Strain	$\lambda^{0.5}$	7.75
Water permeability coefficient	$\lambda^{0.75}$	21.56
Bending stiffness	$\lambda^{4.5}$	100,387,728

The rubble layer consists of Grade 6 crushed stone with a particle size of 13–20 mm. The grain size distribution of the Yamagata sand used for the ground is provided in Fig. 2.

The initial shear modulus (G_0) of the sand layer was calculated using the following equation:

$$G_0 = \rho(v_s)^2, \tag{1}$$

where G_0 is the initial shear modulus, ρ is the mass density of sand, and ν_s is the shear wave velocity of the soil layer.

The pulse method was used to determine the shear velocity of the sand. An impulsive sine wave (amplitude: 100 Gal, period: 0.0176 s) was input at the bottom of the shaking table by the electrohydraulic vibration machine. The acceleration responses at two locations, one at the top of the soil layer and another at the bottom of the layer, were recorded in time-history waves to capture the difference in the peak time between the two locations. Then, the shear wave velocity (ν_s) was calculated

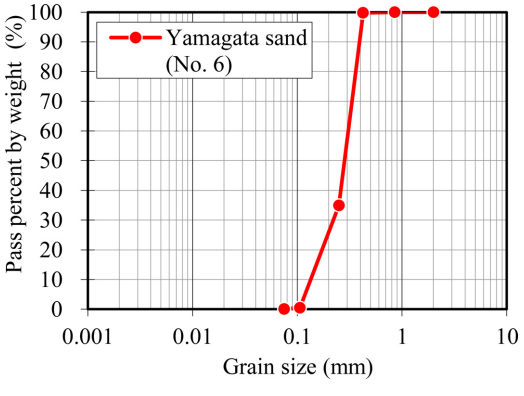

Fig. 2. Grain size distribution of Yamagata sand.

using the following equation:

$$v_s = \frac{H}{\Delta T}, \tag{2}$$

where ν_s is the shear wave velocity, H is the height of the soil layer or distance between the two locations, and ΔT is the difference in the peak time between the two locations.

2.2. *Instrument and deployment*

The accelerometers and pore water pressure transducers were arranged in the near and far-field areas of the ground at various depths of the liquefaction and non-liquefaction layers, shown in Fig. 3. Figure 4 shows the arrangement of accelerometers and acrylic foundation of test model in the soil layers before vibration test. The accelerometers were attached at the top and bottom of the pier. Two horizontal laser displacement transducers were installed at the top and bottom of the pier, and two vertical displacement transducers were installed at the bottom of the pier. The circular targets were embedded in the ground surface to record their movements before and after shaking.

2.3. *Base excitation*

The input ground motion in this vibration test was a base harmonic acceleration with a constant frequency of 10 Hz. The duration time was approximately 2.5 s. The amplitude increased from 50 Gal to 300 Gal, and the case of 50 Gal input ground motion is shown in Fig. 5. The frequency and wave numbers of input ground motion were selected in consideration of the subduction zone earthquakes (level 2 earthquake motion) and the similarity law.

3. Numerical Analysis

ESA using a cocktail glass model was applied in this analysis with the FLIP program (developed by Port and Airport Research, Institute, Yokosuka, Japan). The 2D finite element method model was adopted to simulate the behavior of foundation and soil–structure interaction due to FLIP program is limited by a number of element in 3D simulation and side friction force is assumed to be very small during liquefaction of the ambient loose sand.

3.1. *Calculation model*

The numerical model for the ESA is shown in Fig. 6. The boundary at the bottom of the model was fixed in the vertical and horizontal directions, and the lateral boundary at the two sides was fixed in the horizontal direction. The walls of the SPSP foundation and the acrylic plate at the top of the pier were modeled as elastic beam elements. The steel footing plate, acrylic cap of the piles, and partition walls for

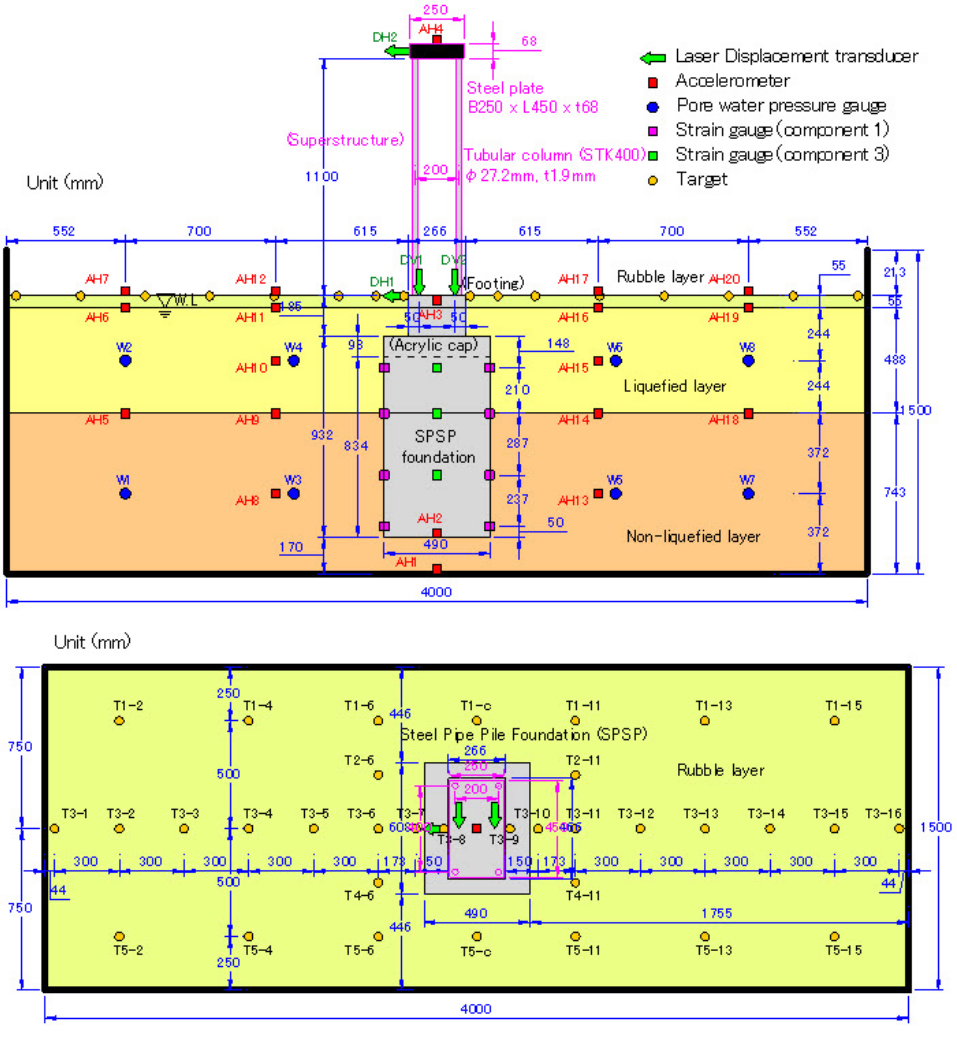

Fig. 3. General view of the experimental model and transducer arrangement.

longitudinal bridge axis were modeled as plane strain elements. The soil was modeled as a plane strain element. Along the soil-wall interface, the walls and adjacent soil elements were connected by a few springs in the vertical and horizontal directions. The horizontal springs were modeled as cut-off tension springs. The thickness of the plane strain element was the same as the width of the test vessel. By modeling the pile in the 2D calculation model, nonlinear spring elements between the pile and the ground are usually adopted to account for soil movement among the piles, or the 3D effect. By modeling the SPSP foundation, side wall friction is accounted for by the spring element. This spring property is the same as that of the vertical spring at the front wall. Figure 6 shows the property of joint between soil and foundation on

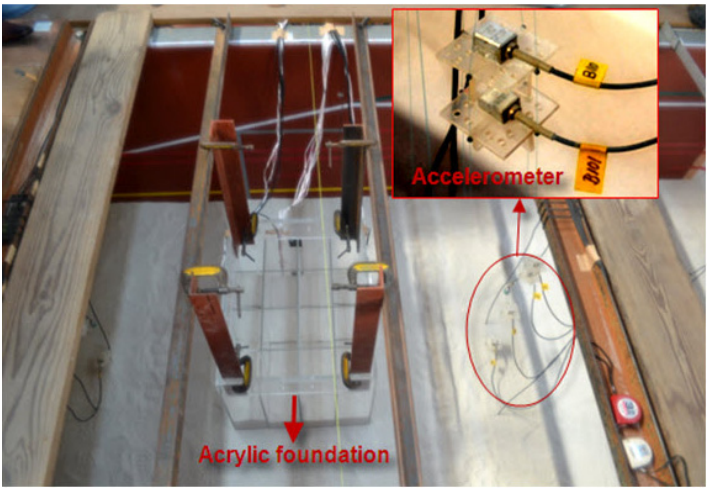

Fig. 4. Installation of accelerometer in the vibration test.

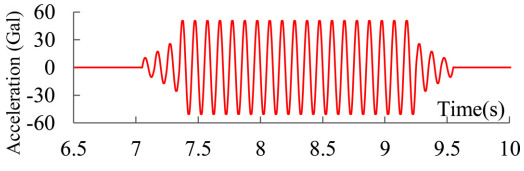

Fig. 5. Acceleration wave input of 50 Gal at the base.

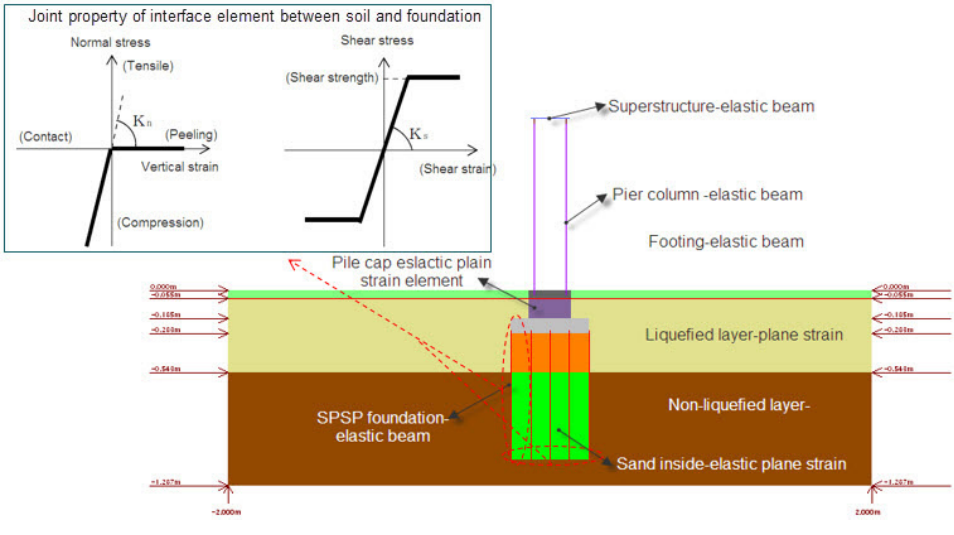

Fig. 6. Numerical model in an ESA using a cocktail glass model.

two sides and at the bottom of foundation. The numerical integration was performed using the Wilson-θ method with $\theta = 1.4$. A Rayleigh damping method with parameters $\alpha = 0$ and $\beta = 0.0002$ was used to ensure the numerical stability of the analysis. In the analysis, the self-weight analysis step was conducted to calculate the initial stress and strain of the model before the calculation of the dynamic analysis.

3.2. *Cocktail glass model*

In the ESA, the boundary condition of pore water in ESA using a cocktail glass model was considered in the undrained conditions (no seepage) at the side walls and bottom wall of the test tank. The numerical model in the analysis is shown in Fig. 6. The influence of stress (or strain) history on the cyclic deformation-strength characteristics of soil in the liquefaction layer is shown in Fig. 7. The figure shows the relationship between stress and strain of the liquefaction layer in both the indoor triaxial vibration test and ESA. The dashed line shows the stress–strain response for a simulation with cyclic stress ratio of 0.23 and vertical effective stress (σ'_v) of 96.3 kPa. The continuous line shows stress–strain response from a typical laboratory test on loose (relative density, D_r, of 50%) Yamagata sand with cyclic stress ratio of 0.23 and vertical effective stress (σ'_v) of 96.3 kPa. The soil was modeled as plane strain elements using the cocktail glass model of the loose sand.

The cocktail glass model is improved from a strain-space multiple-mechanism model in the drained condition suggested by Iai *et al.* [2011], as shown in Fig. 8. There are two primary assumptions in this model. First, the volumetric strain is decomposed into a dilative component and contractive component, as determined in Eq. (3). The dilative component affects the dissipation of pore water pressure in the steady state and the horizontal displacement response. The contractive component can lead to the failure of soil or an increase in the magnitude of the response of soil

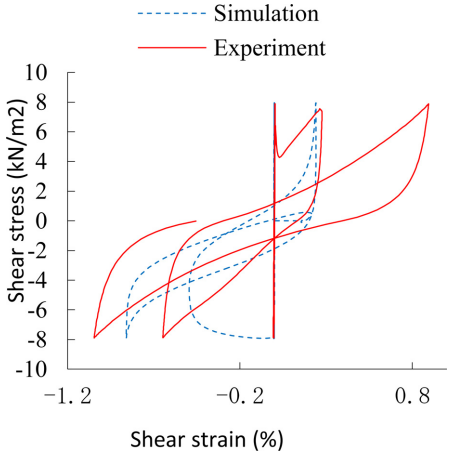

Fig. 7. Stress–strain curve from liquefaction parameters.

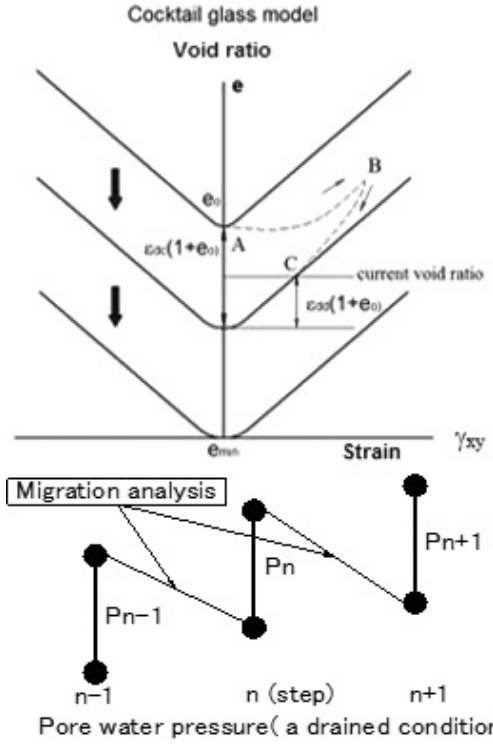

Fig. 8. Cocktail glass model in ESA (suggested by Iai *et al.* [2011]).

movement, whereas the dilative component can limit the magnitude. The division is due to the dilatancy at the minimum void ratio of cohesion-less soil, which makes it impossible to produce a contraction; during the cycle, shear volumetric strain is contractive if cohesion-less soil accumulates non-reversible damages. The curve representing the relationship between the volumetric strain and shear strain is similar to a cocktail glass; hence, it is called a cocktail glass model. The second is a relationship between the relative velocity and the coefficient of permeability determined in Eq. (5). This assumption influences the rate of pore water development and dissipation as follows:

$$\varepsilon_d = \varepsilon_d^c + \varepsilon_d^d, \tag{3}$$

where ε_d is the volumetric strain; ε_d^c is the contractive component; and ε_d^d is the dilative component.

The migration analysis was performed at every calculation step, and pore water pressure decreased, as shown in Fig. 8. Ozutsumi [2003] presented the migration of water obtained by the multi-dimension equation of consolidation by Biot:

$$\{k(\theta)h_i\}_i - \left(\frac{\partial \delta_{i,i}}{\partial t}\right) S_r - C(\psi)\left(\frac{\partial h}{\partial t}\right) = 0, \tag{4}$$

Table 2. List of soil parameters.

	Parameter	Symbol	Liquefaction layer	Non-liquefaction layer	Rubble layer
Parameters for deformation characteristics	Wet unit weight	ρ (t/m^3)	1.96	2.05	1.37
	Initial shear modulus	G_{ma} (kPa)	3,866	21,788	2,993
	Initial bulk modulus	K_{ma} (kPa)	10,083	56,819	7,805
	Standard confining pressure	σ'_{ma} (kPa)	2.27	6.85	0.28
	Poisson's ratio	ν	0.33	0.33	0.33
	Internal friction angle	φ_{f} (degree)	36.55	42.80	41.60
	Hysteretic damping ratio	$h_{\max}$	0.24	0.24	0.24
Parameters for Cocktail glass model	Reduction factor of bulk modulus for liquefaction analysis	r_{K}	0.5	—	—
	Power index of bulk modulus for liquefaction analysis	l_{K}	2	—	—
	Parameter controlling dilative and contractive components	$r_{\varepsilon \mathrm{d}}$	0.2	—	—
	Parameter controlling contractive component	$r^{c}_{\varepsilon \mathrm{d}}$	6.0	—	—
	Parameter controlling initial phase of contractive component	q_1	1	—	—
	Parameter controlling final phase of contractive component	q_2	0.5	—	—
	Limit of contractive component	$\varepsilon_{\mathrm{d}}^{\mathrm{cm}}$	0.5	—	—
	Small positive number to avoid zero confining pressure	S_1	0.005	—	—
	Parameter controlling elastic range for contractive component	c_1	2.5	—	—
	Permeability coefficients	$k_x = k_y$ (m/s)	3.02E-4		

where $k(\theta)$ is the coefficient of permeability; ψ is the pressure head; $C(\psi) = n(\frac{\partial S_r}{\partial \psi})$ is the relative water content; n is the porosity; S_r is the degree of saturation; h is the hydraulic gradient; and δ is the displacement. k is determined by the sand size and the void ratio in the test vessel.

The coefficient of permeability (k) suggested by Chapuis and Aubertin [2003] for sand used in the cocktail glass model is as follows:

$$k = C\frac{g}{\mu_w \rho_w}\frac{e^3}{S^2 D_R^2(1+e)}, \tag{5}$$

where k is the coefficient of permeability; C is the constant; μ_w is the dynamic viscosity of water; ρ_w is the density of water; D_R is the specific weight of sand ($D_R = \rho_s/\rho_w$); ρ_s is density of sand; S is the specific surface; and e is the void ratio.

Parameters for deformation characteristics were obtained by a simplified procedure (Morita *et al.* [1997]). The liquefaction parameters of the soil layers for the cocktail glass model were determined using a trial-error method. Firstly, these parameters were roughly estimated in the limit values (Iai [1991] and Hyodo *et al.* [2008]). Based on these the estimated parameters, the stress–strain hysteresis and liquefaction resistance curves were established in the numerical method. After that, the calibration of these parameters was conducted to coincide between the experiment and simulation (Ichii and Murakami [2017]). The final parameters are summarized in Table 2.

4. Results and Discussions

4.1. *Dynamic responses of the ground*

4.1.1. *Excess pore water pressure (EPWP) and horizontal acceleration*

The time histories of the EPWP at W4 in the near field and W8 in the far field of the experiment and cocktail glass model under the 300-Gal input ground motion are shown in Fig. 9. The generation of pore water pressure began increasing after 7.5 s, and the EPWP reached its maximum value at 9.5 s and immediately dropped after the vibration stopped. This is because the limitation of the 1-G shaking table test. Regarding the shaking table test, the model had smaller dimensions of which geometric scale was reduced by a factor of 60. The undrained condition during shaking did not hold any longer because the time for drainage was reduced by a factor of 60. The dissipation of EPWP in the numerical model occurs very quickly due to the large value of the coefficient of permeability of the test sand and the low value of water viscosity. The numerical method also partly performed the generation of pore water pressure in the vibration test.

Figure 10 presents the EPWP ratios from the 50 Gal to 300-Gal input ground motions for the experiment and the glass cocktail model. The EPWP ratio is increased due to the increase in input ground motion in the cocktail glass model. In the vibration test, the EPWP ratio is increased to 0.7 even though the input ground

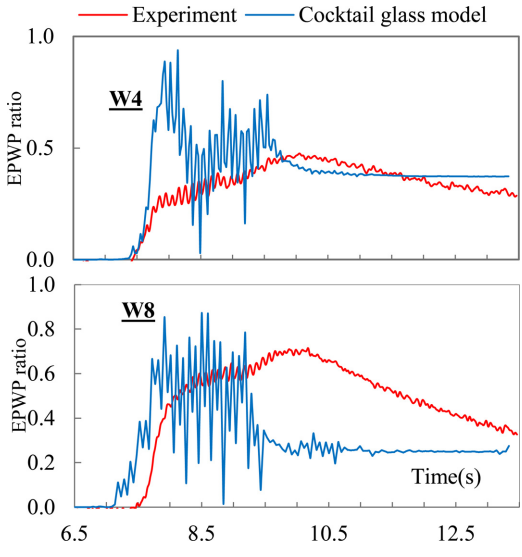

Fig. 9. Time history of EPWP ratio at W4 and W8 in the model using 300 Gal.

motion was 100 Gal. The EPWP ratio at W4 given by the calculation was approximately 0.2. The sand in the liquefied layer in the vessel may have been looser than expected at this point.

The time histories of the horizontal accelerations at points AH8, AH10 and AH19 are shown in Fig. 11. In the non-liquefaction layer, the acceleration at AH8, AH10 and AH19 of the cocktail glass model was in good agreement with that of the experiment, and the acceleration at AH8 in the non-liquefaction layer did not display any amplitude reductions during the shaking period. Meanwhile, the acceleration at the near-field AH10 and far-field AH19 in the liquefaction layer decreased significantly from 7.5 to 10 s, as shown in Fig. 11.

4.1.2. *Vertical displacement*

Figure 12 presents the distribution of the measured residual displacement in the 300 Gal case of the experiment. The figure illustrates that the vertical displacement

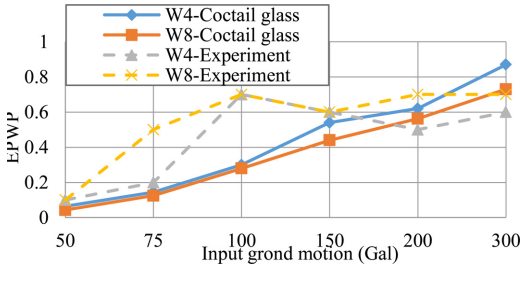

Fig. 10. EPWP ratio in the model from 50 Gal to 300 Gal.

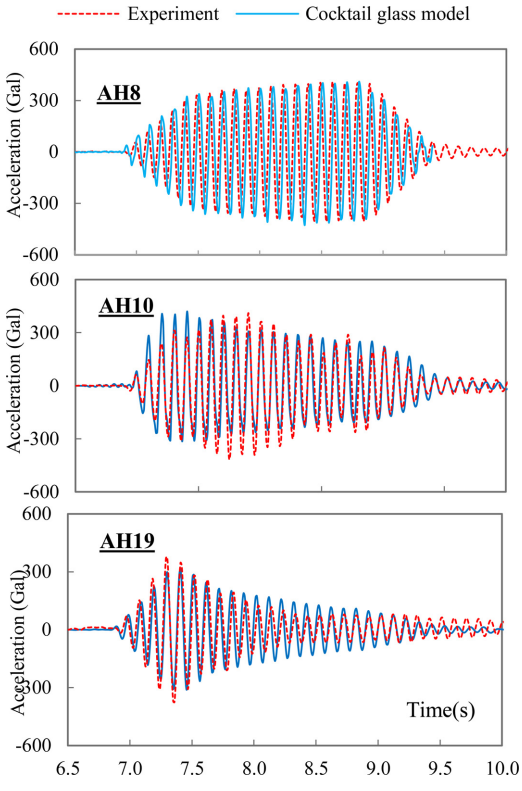

Fig. 11. Time history of horizontal acceleration at AH8, AH10 and AH19 in the model using 300 Gal.

distribution on the surface was quite uniform at approximately 10 mm; however, the displacement of points T3-8 and T3-9 close to the foundation was much larger than that of other points. This behavior may be the result of the interaction between the foundation and the adjacent soil partially failing during shaking. The phenomenon was also explained by the numerical method using a cocktail glass model, as shown in Fig. 13: the displacements at T3-8 and T3-9 were also the largest values compared with the other cases. This figure shows that after the shaking time, the displacement reached a constant value, which is a residual displacement. There was a little difference of residual displacement response between the experiment and simulation. The difference may be due to a limitation of 2D numerical model in performing the movement of soil in two sides of test model during liquefaction in the vibration test. This movement may cause more lateral friction pressure on the foundation structure.

4.2. *Dynamic responses of foundation*

4.2.1. *Horizontal acceleration and horizontal displacement*

Figure 14 presents the time histories of the horizontal acceleration of the superstructure and pile cap of the model under the 300 Gal input ground motion in both

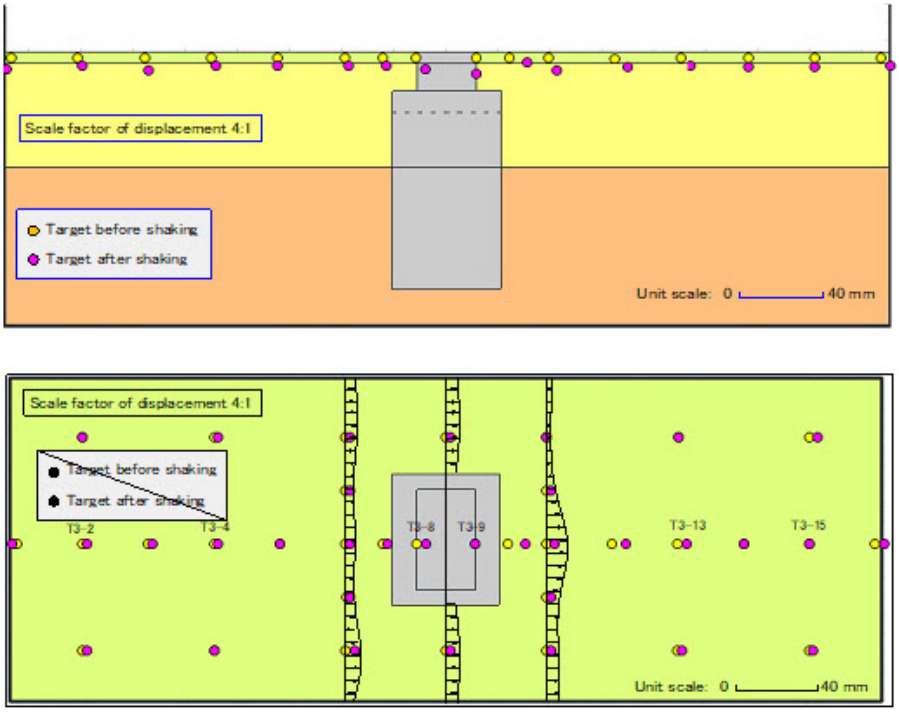

Fig. 12. Measured residual displacement distribution of the ground surface movement under 300 Gal.

the experiment and the numerical methods. For the superstructure, the difference of acceleration at AH4 and AH3 between the experiment and cocktail glass model was insignificant. The acceleration of the experiment was approximately 1.18 times larger for the pile cap at AH3.

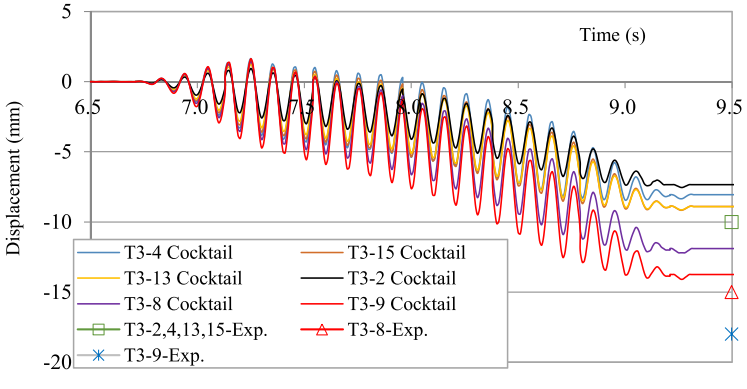

Fig. 13. Time histories of surface vertical displacement at T3-2, 4, 5, 8, 9, 13 and 15 in the numerical model.

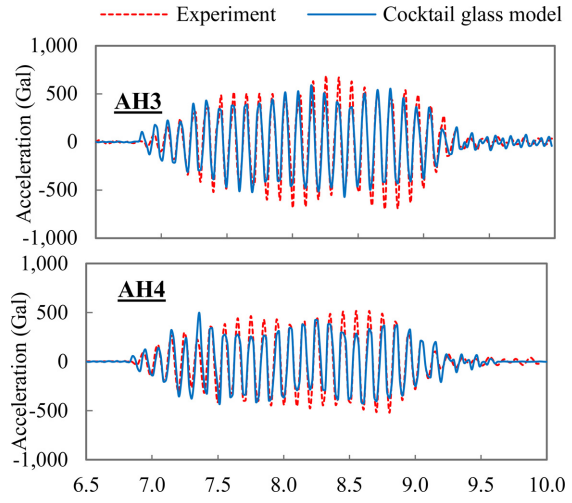

Fig. 14. Time history of horizontal acceleration response of superstructure and pile cap of 300 Gal.

Figure 15 presents the time histories of the horizontal displacements of the pile cap and superstructure in the model in both the experiment and the cocktail glass model. The displacements at DH1 and DH2 in the experiment were larger than those in the cocktail glass model. This is because the pore water pressure in the numerical method more rapidly dropped than the experiment during liquefaction as shown in Fig. 9. A residual displacement was observed in the experiment and numerical methods. The residual displacement was caused by a lateral spreading movement during liquefaction, and the foundation works not only as a supporting pier but

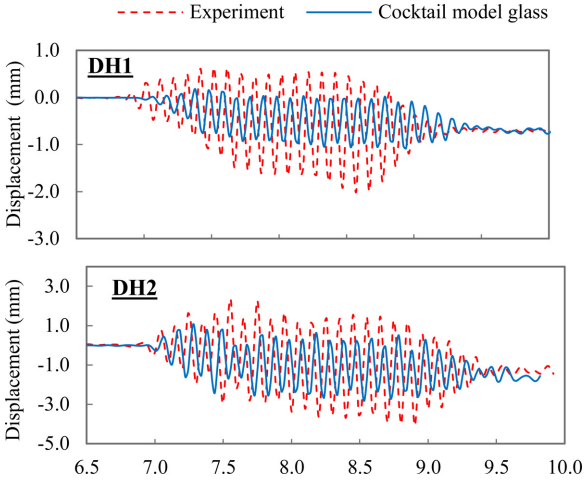

Fig. 15. Time history of horizontal displacement response of superstructure and pile cap of 300 Gal.

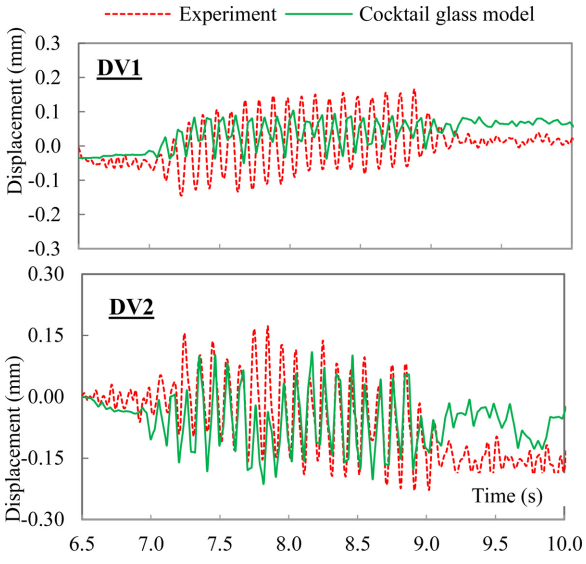

Fig. 16. Time history of vertical displacement response of pile cap under 300 Gal.

also as a retaining wall. Therefore, the lateral pressure of the soil becomes more significant.

4.2.2. *Vertical displacements of foundation*

Figure 16 shows that the vertical displacement at DV1 and DV2 in the 300 Gal case in the experiment was approximately 1.18 times larger than the displacements in the cocktail glass model. A residual displacement was also clearly observed in both the experiment and the numerical methods. In addition, compared with the vertical displacement of surrounding ground, the residual displacement of the foundation is very small. The displacement is minimal because the foundation was inserted into the non-liquefaction layer, which restrained the vertical movement of the foundation. Moreover, the embedment of foundation in the non-liquefaction also restrained the horizontal displacement of foundation as shown in Fig. 15.

Figure 17 presents a comparison of the residual vertical displacement of the foundation between the experiment and the cocktail glass model from 50 Gal to 300 Gal. Each color point is a comparison value between DV1 and DV2 corresponding with a case of input ground motion. These values gradually increased, demonstrating that the displacements increased due to the increase of input ground motion. Additionally, the displacements in the cocktail glass model were approximately 1.2 times less than those in the experiment for all input ground motion cases.

Based on Eq. (6), the inclination of the foundation was 0.25% in the experiment and was 0.17% in the numerical methods. Therefore, the settlement of the foundation was inclined in both cocktail glass model and experiment.

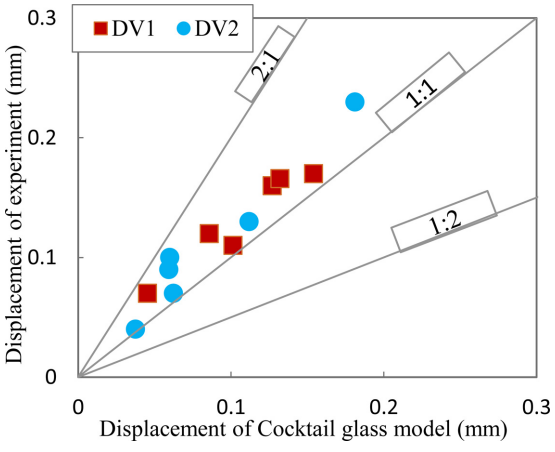

Fig. 17. Comparison of residual vertical displacement at pile cap between the experiment and the cocktail glass model from 50 Gal to 300 Gal.

The inclination of the foundation was determined by the following equation:

$$\alpha = \frac{\mathrm{DV2} - \mathrm{DV1}}{L} 100, \tag{6}$$

where α is the inclination of the foundation (%); DV1 and DV2 are the residual values of vertical displacements at the top of the footing (mm); and L is the distance between DV1 and DV2 (266 mm).

4.3. *Various permeability coefficients*

The study did not consider the variation of permeability with the build-up of pore water pressure. Arulanandan and Sybico [1992] demonstrated that the permeability values during the initial liquefaction play an important role in post-liquefaction settlement analysis. Therefore, due to the limitations of the numerical method, the study used only the initial permeability coefficient as a constant value in the calculation process.

The ESA was conducted on three cases with various permeability coefficients to investigate the effect of this coefficient on the settlement of the SPSP foundation and the surrounding ground, as shown in Table 3.

Table 3. Study cases of permeability coefficients in the ESA.

Items	Permeability coefficient, k (m/s)	Note
Case 1	3.02×10^{-4}	The coefficient was determined from the sand properties of liquefaction layer
Case 2	1.0×10^{-4}	A case study
Case 3	1.0×10^{-4}	A case study in an exceedingly small permeability condition

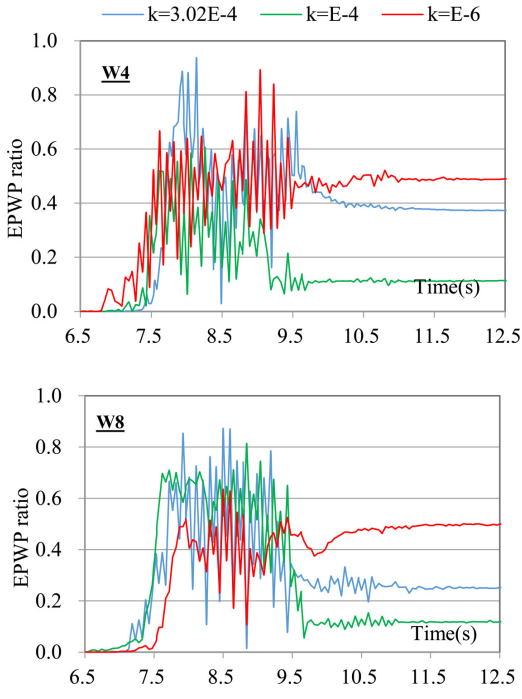

Fig. 18. Time history of EPWP ratio at W4 and W8 in the model under 300 Gal in the case of $k = 3.03$E-4, E-4 and E-6.

Time histories of the pore water pressure ratio at W4 and W8 under 300-Gal input ground motion in case of permeability coefficient $k = 3.02$ E-4, E-4 and E-6 are shown in Fig. 18. The pore water pressures quickly began dissipating after a shaking time of 2 s and immediately approached constant values. In the case of permeability coefficient $k =$ E-6, the peak values of the EPWP ratio time history did not decrease during shaking compared to other cases, demonstrating that the liquefaction time of the soil layer in the case of a lower permeability coefficient was longer than that of other cases. In particular, during post-liquefaction, the EPWP ratio of the coefficient $k =$ E-6 was much higher than it was in other cases. The EPWP ratio in the case of coefficient $k =$ E-4 was also higher than it was in the case of $k = 3.02$E-4 at point W8, but it was almost the same at point W4; this result was observed in both the W4 and W8 time history of the EPWP ratio in Fig. 18. As a result, in the case of the lower permeability coefficient, the pore water has difficulty dissipating and results in a higher EPWP ratio in the post-liquefaction state.

Figures 19 and 20 present the time histories of vertical displacement at DV1 of the pile cap and at T3-4 of the surrounding ground under 300 Gal for three different permeability coefficients. The residual displacement of the lowest permeability coefficient case was less than it was in other cases. This phenomenon is observed in both the DV1 of the foundation and the T3-4 of the ground. Therefore, it demonstrates

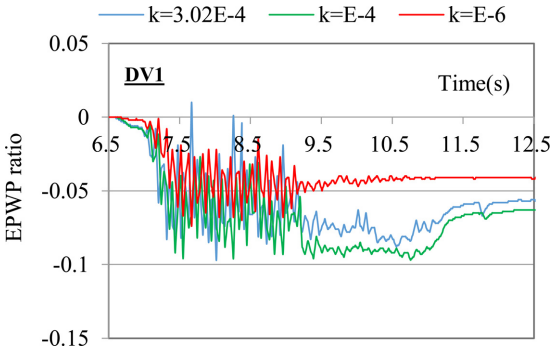

Fig. 19. Time history of vertical displacement at DV1 of pile cap under 300 Gal in case of k = 3.03E-4, E-4 and E-6.

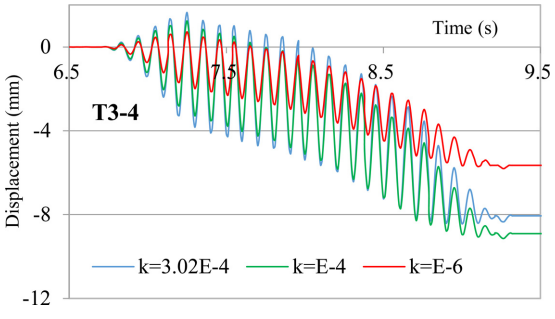

Fig. 20. Time history of vertical displacement at T3-4 of ground under 300 Gal in case of k = 3.03E-4, E-4 and E-6.

that the settlement of the foundation and ground increases as the permeability coefficient increases.

5. Conclusions

Numerical analysis using a cocktail glass model and a shaking table test were conducted on an SPSP foundation to investigate the effect of the settlement of surface ground and SPSP foundation during liquefaction. The primary findings are as follows:

(1) In low-amplitude input ground motion, the settlement of the foundation is minimal. In cases of higher-amplitude input, when the liquefaction is observed, the settlement of the foundation quickly increases; however, compared to the settlement of the ground, this settlement is very small due to the foundation being inserted into the non-liquefaction layer, which restrained the movement of the foundation.

(2) The inclined settlement of SPSP foundations appeared to be significant during post-liquefaction due to the effect of lateral spreading movement in the liquefaction stage. This result was clearly observed in the shaking table test.
(3) ESA, using a cocktail glass model that considers the dilative component of the sand and seepage of water, can be used to model seismic responses of SPSP foundation, particularly to estimate the dissipation of the pore water pressure ratio and the settlement of the foundation and the surrounding ground.
(4) The settlement of the surface ground and the SPSP foundation is significantly influenced by the permeability coefficient. The higher the permeability coefficient is, the larger the settlement during liquefaction.

Acknowledgment

The authors gratefully acknowledge experimental support from the Penta-Ocean Construction Corporation in Japan for the use of their 1-G shaking table facility.

References

Alchamaa, R. [2010] "Analysis of post-liquefaction deformation of ground associated with seepage due to excess pore water pressure dissipation after earthquake," Dissertation, Tokyo Metropolitan University Institutional Repository.

Arulanandan, K. and Sybico, J. Jr. [1992] "Post-liquefaction settlement of sand," *Proc. Wroth Memorial Symp.*, Oxford University, England.

Cetin, K. O., Bilge, T. H., Wu, J., Kammarer, M. A. and Seed, R. B. [2009a] "Probabilistic models for cyclic straining of saturated clean sands," *J. Geotechn. Geo-Environ. Eng.* **135**(3), 371–386.

Cetin, K. O., Bilge, T. H., Wu, J., Kammarer, M. A. and Seed, R. B. [2009b] "Probabilistic model for the assessment of cyclically induced reconsolidation settlements," *J. Geotechn. Geo-Environ. Eng.* **135**(3), 387–398.

Chapuis, R. P. and Aubertin, M. [2003] "Predicting the coefficient of permeability of soil using Kozeny-Carman equation," Technical report, EPM-RT-2003-3.

Hyodo, J., Iai, S., Yokoyama, N., Ozutsumi, O. and Yoshikawa, S. [2008] "Effective stress analysis considering steady state of sandy soil on centrifuge model test," *The 43rd JGS National Conf.*, pp. 1807–1808 (in Japanese).

Iai, S. [1988] "Similitude for shaking table tests on soil-structure model in 1G gravitational field," *Rept. Port Harbor* **27**(3), 3–24.

Iai, S. [1991]. "A strain space multi mechanism model for cyclic behavior of sand and its application," Report of Earthquake Engineering Research, Note No. 43.

Iai, S., Tobita, T., Ozutsumi, O. and Ueda, K. [2011] "Dilatancy of granular materials in a strain space multiple mechanism model," *Int. J. Numer. Anal. Methods Geomech.* **35**, 360–390.

Ichii, K. and Murakami, T. [2017] "An index on the appropriateness of parameter determination for analysis considering liquefaction. Geotechnical Hazard Mitigation: Experiment, Theory and Practice," *Proc. 5th Int. Conf. on Geotechnical Engineering for Disaster Mitigation and Rehabilitation*, pp. 89–98.

Ishihara, K. and Yoshimine, M. [1992] "Evaluation of settlements in sand deposits following liquefaction during earthquakes," *Soils Found.* **32**(1), 173–188.

Kawakami, F. and Asada, A. [1966] "Damage to the ground and earth structures by the Niigata earthquake of June 16, 1964," *Soils Found.* **6**(1), 14–30.

Kim, S. R., Hwang, J. I., Ko, H. Y. and Kim, M. M. [2009] "Development of dissipation model of excess pore pressure in liquefied sandy ground," *J. Geotechn. Geo-Environm. Eng.* **135**(4), 544–554.

Morita, T., Iai, S., Liu, H., Ichii, K. and Sato, Y. [1997] "Simplified method to determine parameter of FLIP," Technical note of the Port and Harbour research institute, Ministry of Transport, Japan, No. 869 (in Japanese).

Ozutsumi, O. [2003] "Study on numerical analysis method of earthquake damage prediction for ground-structure system on liquefied layer," Doctoral dissertation, Kyoto University (in Japanese).

Shahir, H., Pak, A., Taiebat, M. and Jeremic, B. [2012] "Evaluation of variation of permeability in liquefiable soil under earthquake loading," *Comput. Geotech.* **40**, 74–88.

Shamoto, Y., Zhang, J. M. and Tokimatsu, K. [1998] "Methods for evaluating residual post liquefaction ground settlement and horizontal displacement," *Soils Found.* **2**(2), 69–83.

Tokimatsu, K. and Seed, H. B. [1984] "Simplified procedures of the evaluation of settlements in clean sands" Report No. UCB/GT-84/16, University of California, Berkeley, California.

Tokimatsu, K. and Seed, H. G. [1987] "Evaluation of settlements in sands due to earthquake shaking," *J. Geotechn. Eng.* **113**(8), 861–878.

Trung, N. T., Kiyomiya, O. and Yoshida, M. [2014] "The dynamic behavior of a steel pipe sheet pile foundation in a liquefied layer during an earthquake," *J. Struct. Eng./Earthqu. Eng. Appl. Mech.* **2**, 116–135.

Ueda, K., Tobita, T. and Iai, S. [2008] "A numerical study of dynamic behavior of a self-supported sheet pile wall," *Proc. 14th World Conf. on Earthquake Engineering*, Beijing, China.

Wang, M. W., Li, L. and Han, J. P. [2008] "Effective stress analysis of seismic behaviors of inclined micro-piles on liquefiable soils," *Proc. 14th World Conf. on Earthquake Engineering*, Beijing, China.

Wang, B., Zen, K., Chen, G. Q. and Kasama, K. [2011] "Effect of permeability of liquefaction-induced lateral flow in shaking table tests," *Proc. Int. Conf. on Coastal Structures*, Yokohama, Japan.

Wu, J. and Seed, R. B. [2004] "Estimation of liquefaction-induced ground settlement (case studies)," *Proc. 5th Int. Conf. on Case Histories in Geotechnical Engineering*, New York, NY, USA, April 13–17.

Yoneda, M. [1990] "On the longitudinal motion of girder of cable stayed bridges and simplified method of estimating natural frequency corresponding to this motion," *J. Struct. Mech. Earthq. Eng.* **7**, I-4. (in Japanese).

Yoshida, M., Mitou, M., Kiyomiya, O., Tashiro, S. and Gouda, S. [2012] "Effect of seismic reinforcement of sheet pile quay wall using ground anchor," *Proc. 15th World Conf. on Earthquake Engineering*. Lisbon, Portugal.